SUPPLEMENTAL MATERIAL

S1. Data and Method: Statistical Analysis on Detrital Zircons Data

Detrital zircons U-Pb dating and trace element composition were compiled from 103 detrital rock samples from various continents and cratons (e.g., Yilgarn, Jack Hills in Australia, White Sea, Urals, Tibet, Himalaya, S. China, Yangtze River, Danube River, India, Indochina in Eurasia, Wyoming, Gulf of Mexico, Acasta in N. America, Brazilian shield in S. America, Antarctica; most of the data were compiled in Balica et al., 2020 to which were added several references published since then. Raw data and associated references can be found in the Supplementary Material Table S1). We filtered out metamorphic zircons based on zircon Th/U ratios (n = 6305 data after filtering; 16% of zircon data were rejected). These zircons are expected to have formed in magmatic or high-grade granulitic conditions, derived from intermediate to felsic rocks (with median Th/U value at 0.6; see Rubato et al., 2002; Kirkland et al., 2015). We focused here on the Eu anomaly in zircon (noted Eu*/Eu and calculated as $Eu_N/((Sm_N+Nd_N)/2)$; the N stands for normalization to chondrite reference values from Barrat et al. (2012), see the data table in Supplementary Material Table S1). The timeseries is built using a similar bootstrap approach as in Dhuime et al. (2012). In this study, a 500 Ma wide rolling window was used (with a 20 Ma rolling step through the data) as it allows to highlight major and long-term change in zircon signature. A bootstrap analysis is performed on data included in each time window, extracting basic statistics including median value, 99.5% and 0.5% percentile boundary values, average value, standard deviation at each iteration (n of iterations = 500). The peak of the distribution of bootstrapped median data and 1 and 3 sigma s.d. range are calculated and displayed as a timeseries in figure 1 of the manuscript. The python script used for this statistical treatment is available in the Supplementary Material S3.

Balica, C., Ducea, M. N., Gehrels, G. E., Kirk, J., Roban, R. D., Luffi, P., Chapman, J.B., Triantafyllou, A., Guo, J., Stoica, A.M., Ruiz, J., Balintoni, I., Profeta, L., Hoffman, D. & Petrescu, L. (2020). A zircon petrochronologic view on granitoids and continental evolution. Earth and Planetary Science Letters, 531, 116005. https://doi.org/10.1016/j.epsl.2019.116005

Barrat, J. A., Zanda, B., Moynier, F., Bollinger, C., Liorzou, C., & Bayon, G. (2012). Geochemistry of CI chondrites: Major and trace elements, and Cu and Zn isotopes. Geochimica et Cosmochimica Acta, 83, 79-92. https://doi.org/10.1016/j.gca.2011.12.011

Dhuime, B., Hawkesworth, C. J., Cawood, P. A., & Storey, C. D. (2012). A change in the geodynamics of continental growth 3 billion years ago. Science, 335(6074), 1334-1336. https://doi.org/10.1126/science.1216066

Kirkland, C. L., Smithies, R. H., Taylor, R. J. M., Evans, N., & McDonald, B. (2015). Zircon Th/U ratios in magmatic environs. Lithos, 212, 397-414. https://doi.org/10.1016/j.lithos.2014.11.021

Rubatto, D. (2002). Zircon trace element geochemistry: partitioning with garnet and the link between U–Pb ages and metamorphism. Chemical geology, 184(1-2), 123-138. https://doi.org/10.1016/S0009-2541(01)00355-2 .

S2. Phase Equilibria Modelling

Petrological modelling has been performed to discuss the role of magma sources, pressure, temperature conditions (*P-T*), stable mineral phases and hydration state. Calculations were done with Theriak–Domino software (de Capitani et al., 2010), and the internally consistent thermodynamic data set of Holland and Powell (ds62; revised in 2011). All petrological calculations were performed in the Na_2O–CaO–K_2O–FeO–MgO–Al_2O_3–SiO_2–H_2O–TiO_2–O_2 (NCKFMASHTO) compositional system using average mafic composition from Keller and Schoene (2012). Three linearized geotherms (at 35, 50 and 100°C/kbar) are added on the calculated phase diagrams to represent the ranges of thermal gradients from Archean to modern tectonics (Brown, 2014). The H_2O content was fixed to allow minimum water-saturation at the initial melting point along each geotherm (see modelled compositions in Supplementary Material DR2). Calculations also consider melt loss events (MLE) occurring when the melt reaches a threshold of 7 vol.% (MLE-a) and 20 vol% (MLE-b). These volume thresholds are two endmembers and were chosen based on studies investigating molten amphibolites and felsic magma rheology (Diener et al. 2014; Bowman et al., 2021 for MLE-a and Rushmer, 1995; Vigneresse et al., 1996 for MLE-b and references therein). All calculations considered activity–composition (a–x) relations for intermediate/tonalitic melt, augite clinopyroxene, and clinoamphibole (Green et al., 2016); plagioclase and K-feldspar (Holland and Powell, 2003); paragonite-muscovite (White et al., 2014); orthopyroxene, garnet, biotite, and chlorite (White et al., 2014); magnetite–spinel, ilmenite–hematite (White et al., 2002 and White et al., 2000 respectively); olivine and epidote (Holland and Powell, 2011). Pure phases included quartz, rutile, titanite, albite, and aqueous fluid (H_2O). We do not consider MnO in the compositional system as the a-x relations used for tonalitic melt, clinopyroxene, and clinoamphibole do not incorporate this component. A python code was developed to draw pseudosection and fill PT field with system's variance (see all python codes in Supplementary Material DR5). The Fe3+/ΣFe ratio in the system was fixed to that reported within the range of estimated values for modern-day and Archean oceanic basalts: 0.22 and 0.12 respectively (Condie, 1981; Bézos et al., 2005).

For Figure 3 in the manuscript, a new python code has been developed to wrap Theriak-Domino tasks to run modelling iteratively for different mafic systems through time (see all python codes in Supplementary Material S3). Timeseries in figure 3 show modelled volumetric proportions of garnet and plagioclase phases at melt loss event B (20 vol.% of melt produced), under minimum water-saturation conditions, along the 100°C/kbar geotherm and using successive average mafic composition for each 100 Myr step (in the NCKFMASHTO chemical system; see Keller and Schoene, 2012 compilation in Suppl. Mat. Table S2 and Text S2). Error bars for each point is a propagated uncertainty from the one estimated for the mafic source composition (see Keller and Schoene, 2012). In order to estimate the impact of water saturation on plagioclase modal proportion, we also run the code considering a fixed 5 wt% H_2O (water saturation) in the mafic source for the post-1 Ga period. This code also displays TX phase diagram.

Bézos, A., & Humler, E. (2005). The Fe3+/ΣFe ratios of MORB glasses and their implications for mantle melting. Geochimica et Cosmochimica Acta, 69(3), 711-725. https://doi.org/10.1016/j.gca.2004.07.026

Bowman, E. E., Ducea, M. N., & Triantafyllou, A. (2021). Arclogites in the subarc lower crust: effects of crystallization, partial melting, and retained melt on the foundering ability of residual roots. Journal of Petrology, 62(12), egab094. https://doi.org/10.1093/petrology/egab094

Brown, M. (2014). The contribution of metamorphic petrology to understanding lithosphere evolution and geodynamics. Geoscience Frontiers, 5(4), 553-569. https://doi.org/10.1016/j.gsf.2014.02.005

Condie, K. C. (1981). Archean greenstone belts. Elsevier.

de Capitani, C., & Petrakakis, K. (2010). The computation of equilibrium assemblage diagrams with Theriak/Domino software. American mineralogist, 95(7), 1006-1016. https://doi.org/10.2138/am.2010.3354

Diener, J. F., & Fagereng, Å. (2014). The influence of melting and melt drainage on crustal rheology during orogenesis. Journal of Geophysical Research: Solid Earth, 119(8), 6193-6210. https://doi.org/10.1002/2014JB011088

Green, E. C. R., White, R. W., Diener, J. F. A., Powell, R., Holland, T. J. B., & Palin, R. M. (2016). Activity–composition relations for the calculation of partial melting equilibria in metabasic rocks. Journal of metamorphic Geology, 34(9), 845-869. https://doi.org/10.1111/jmg.12211

Holland, T. J. B., & Powell, R. (2011). An improved and extended internally consistent thermodynamic dataset for phases of petrological interest, involving a new equation of state for

solids. Journal of metamorphic Geology, 29(3), 333-383. https://doi.org/10.1111/j.1525-1314.2010.00923.x

Holland, T., & Powell, R. (2003). Activity–composition relations for phases in petrological calculations: an asymmetric multicomponent formulation. Contributions to Mineralogy and Petrology, 145(4), 492-501. https://doi.org/10.1007/s00410-003-0464-z

Keller, C. B., & Schoene, B. (2012). Statistical geochemistry reveals disruption in secular lithospheric evolution about 2.5 Gyr ago. Nature, 485(7399), 490-493. https://doi.org/10.1038/nature11024

Rushmer, T. (1995). An experimental deformation study of partially molten amphibolite: Application to low-melt fraction segregation. Journal of Geophysical Research: Solid Earth, 100(B8), 15681-15695. https://doi.org/10.1029/95JB00077

Vigneresse, J. L., Barbey, P., & Cuney, M. (1996). Rheological transitions during partial melting and crystallization with application to felsic magma segregation and transfer. Journal of Petrology, 37(6), 1579-1600. 10.1093/petrology/37.6.1579

White, R. W., Powell, R., & Clarke, G. L. (2002). The interpretation of reaction textures in Fe-rich metapelitic granulites of the Musgrave Block, central Australia: constraints from mineral equilibria calculations in the system K2O–FeO–MgO–Al2O3–SiO2–H2O–TiO2–Fe2O3. Journal of metamorphic Geology, 20(1), 41-55. https://doi.org/10.1046/j.0263-4929.2001.00349.x

White, R. W., Powell, R., Holland, T. J. B., Johnson, T. E., & Green, E. C. R. (2014). New mineral activity–composition relations for thermodynamic calculations in metapelitic systems. Journal of Metamorphic Geology, 32(3), 261-286. https://doi.org/10.1111/jmg.12071

S3. Link to GitHub Repository for Python Codes

Pure python code to perform bootstrap analysis and plotting trace element timeseries of zircon data. Link to GitHub repository: https://github.com/antoinetri/zircon_petrochro_timeseries (all libraries and requirements are commented in the code and described in the readme file).
Pure python code to wrapper Theriak-Domino thermodynamic calculations and to help at displaying P-T phase diagram (or pseudosection) as a .eps file (the latter is still work in progress, contributions for improvement are welcome). Link to GitHub repository: https://github.com/antoinetri/TheriakDomino_wrappers (all libraries and requirements are commented in the code and described in the readme file).

Figure S1

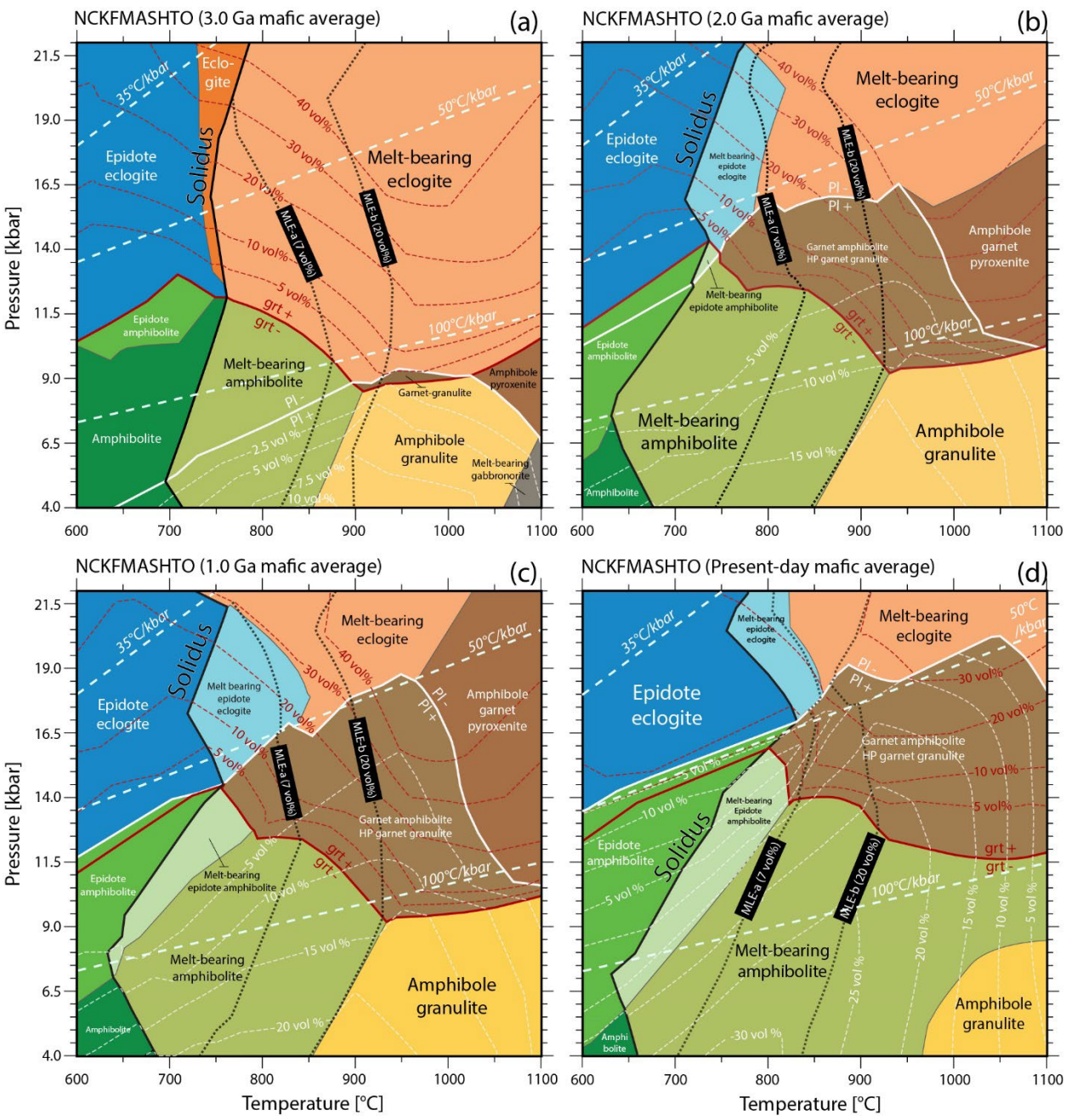

Figure S1 Calculated *P–T* phase diagram (lithological) for mafic crust composition at 3.0 Ga (a), 2.0 Ga (b), 1.0 Ga (c) and present-day (d) in the NCKFMASHTO chemical system (see Suppl. Mat. S2 for details on thermodynamic modelling). These diagrams show the effects of cogenetic phases on melt composition. Two melt loss events (MLE) are shown at 7 and 20 vol% of melt (black dashed lines). Geotherms are displayed as bold dashed white lines and phases proportions in vol.% as light dashed lines in red for garnet (grt) and in white for plagioclase (Pl).

Figure S2

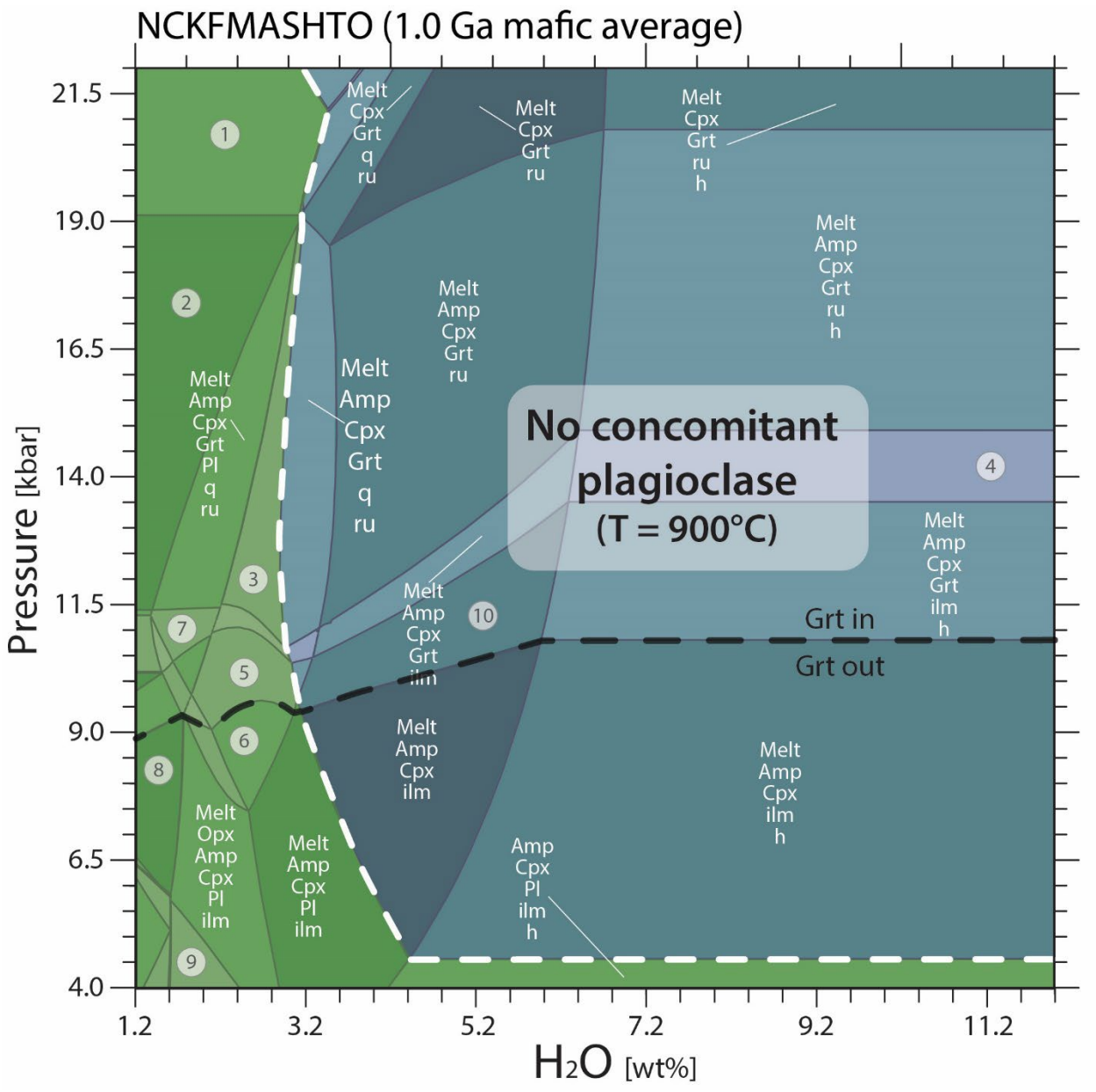

Figure S2. P-X_{H2O} phase diagram using the 1.0 Ga average mafic composition at a constant T condition (T = 900°C) in the NCKFMASHTO chemical system, showing the effects of water content on melt cogenetic phases (i.e. plagioclase stability; see Table S2 and Text S2).